PHYSICAL REVIEW B **95**, 161110(R) (2017)

Thermomechanical stabilization of electron small polarons in $SrTiO_3$ assessed by the quasiharmonic approximation

Mostafa Youssef,[1,2] Bilge Yildiz,[1,2,*] and Krystyn J. Van Vliet[1,3,†]

[1]*Department of Materials Science and Engineering, Massachusetts Institute of Technology, 77 Massachusetts Avenue, Cambridge, Massachusetts 02139, USA*

[2]*Department of Nuclear Science and Engineering, Massachusetts Institute of Technology, 77 Massachusetts Avenue, Cambridge, Massachusetts 02139, USA*

[3]*Department of Biological Engineering, Massachusetts Institute of Technology, 77 Massachusetts Avenue, Cambridge, Massachusetts 02139, USA*

(Received 10 August 2016; revised manuscript received 13 February 2017; published 20 April 2017)

We predict a predominance diagram for electron defects in the temperature-hydrostatic stress space for $SrTiO_3$ by combining density functional theory and the quasiharmonic approximation. We discovered two regimes where small polarons dominate: under tensile stress at lower temperature due to a larger relaxation volume of the defect Ω, and under compressive stress at higher temperature due to a smaller Ω and larger formation entropy. This provides a means to modulate the electronic conductivity via controlling the underlying charge carrier. Furthermore, the results challenge the common association between larger Ω and charge localization by demonstrating that at high temperature the free electron can induce larger Ω compared to the small polaron. This finding is attributed to the ability of the free electron to generate greater vibrational entropy upon finite isothermal expansion.

DOI: 10.1103/PhysRevB.95.161110

An electron can move freely in a periodic crystal unless the lattice is polarizable, in which case the electron can begin to exhibit localization by deforming surrounding ions to form a so-called large polaron. Assisted by lattice vibrations, electron localization can become enhanced to be self-trapped on a single ion. The latter is termed a small polaron or a self-trapped electron. While large polarons traverse crystals in a rapid bandlike fashion, small polarons tend to hop slowly from one ion to the next [1]. Holstein predicted that in a given polarizable crystal, a transition from large to small polaron behavior occurs as the temperature increases above half the Debye temperature Θ_D [2]. Understanding and controlling the extent of electron localization in the family of metal oxides underpins their performance in various applications. For example, delocalization is desired for increasing the electronic conductivity of oxides that function for water splitting and CO_2 reduction [3]. On the other hand, the ease of creating oxygen vacancies in reducible metal oxides is generally correlated with localizing electrons on neighboring host cations; that is, reducing them [4–6]. Temperature and stress are readily available thermodynamic forces to tune the degree of localization of electronic defects. In this Rapid Communication, we reveal how the localization of electron polarons in the metal oxide $SrTiO_3$ is controlled by these forces, primarily via changes in relaxation volume of electronic defects with temperature and pressure.

Strontium titanate ($SrTiO_3$) is an archetype of the versatile perovskite oxides family. The electronic defects (electrons and holes) of bulk $SrTiO_3$ give rise to desirable properties not possessed by the underlying perfect crystal such as superconductivity [7], ferromagnetism [8], and blue-light luminescence [9]. Thus, extensive experimental [10–14] and theoretical [15–17] works have probed the degree of localization of electronic defects in $SrTiO_3$. Experiments have indicated that both large [10,11] and small [12,13] electron polarons can exist or even coexist [14] in bulk $SrTiO_3$. These experiments were rationalized [16] by suggesting that in the dilute limit (i.e., less than 1% defect per unit cell) large polarons prevail, and at higher doping concentrations small polarons prevail. Density functional theory (DFT) calculations at temperature 0 K consistently predict the predominance of free electrons over small polarons [15,16], where it is noted that free electrons are the accessible representation of large polarons in DFT calculations.

Notwithstanding these meticulous studies, we still lack a clear thermodynamic description of the electronic defects in $SrTiO_3$ and in metal oxides in general. For example, $SrTiO_3$ does not adhere [10] to the Holstein prediction [2] of a transition from large to small polaron behavior at $\Theta_D/2$. Moreover, the relaxation volumes for polarons have not been reported experimentally for $SrTiO_3$ and are challenging to obtain theoretically for any charged defect in a semiconductor [18,19]. The relaxation volume of a defect Ω is the change in crystal volume upon attaining full relaxation including this defect. This quantity is fundamental because it both dictates the chemical expansivity [19,20] and is related directly to the absolute deformation potentials of the conduction and valence bands in the case of free electrons and holes, respectively [18,19]. Finally, it is well established that mechanical stresses and strains can substantially alter the concentration [21,22] and mobility of both ionic [23] and electronic defects [24] in semiconductors and insulators. In spite of this, there are few reported studies examining the effects of mechanical stress on the degree of localization of the electronic defects [25]. For example, DFT calculations at 0 K [17] indicated that tensile hydrostatic stress facilitates hole self-trapping in perovskite titanates based on energetic rather than enthalpic considerations. It is not clear whether this prediction holds

*Corresponding author: byildiz@mit.edu
†Corresponding author: krystyn@mit.edu

when the enthalpy of self-trapping is explicitly computed at 0 K.

In this Rapid Communication we combine density functional theory and the quasiharmonic approximation (QHA) to depict the thermodynamic stability of small and large polarons in the temperature T–pressure P space for $SrTiO_3$. This coupling between DFT and QHA has been applied successfully by others to sample finite T and P effects and quantum-mechanical zero-point energies for perfect crystals [26,27] and defects in metals [28]. However, to our knowledge, employing DFT and QHA to quantitatively decipher the coupled effect of thermodynamic forces (T and P) on a charged defect in a semiconductor has not been reported previously. We identified two stability zones for the small polarons in the T-P space: at low T under tensile stress and at high T under compressive stress. In the first zone, the predominance of small polarons is attributable to the larger Ω of this defect, as compared with free electrons. In the second zone, a combination of smaller Ω and larger formation entropy stabilize the small polaron. The unexpectedly larger Ω for the free electron at high T is attributed to its ability to generate more vibrational entropy upon finite isothermal expansion.

DFT calculations were conducted using the projector-augmented plane-wave (PAW) method [29,30] as implemented in VASP code [31–34]. The exchange correlation was described using the revised Perdew, Burke, and Ernzerhof functional for solids [35] equipped with on-site Coulomb interaction terms U [36] on Ti $3d$ states and on O $2p$ states. Following the approach of Ref. [17], we determined that $U_{\mathrm{Ti}} = 5\,\mathrm{eV}$ and $U_{\mathrm{O}} = 8\,\mathrm{eV}$ achieve a near piecewise linearity in the total energy as a function of fractional occupation between unfilled and filled polaronic states on Ti and O, respectively [37]. To describe the stability of small polarons vs free electrons (the latter are a DFT accessible representation of large polarons), we define the Gibbs free energy of self-trapping of the electron polaron on a Ti cation as

$$G_{\text{self-trap}}(T,P) = G_{\text{small}}(T,P) - G_{\text{free}}(T,P), \qquad (1)$$

where G_{small} and G_{free} are the Gibbs free energies of the defective crystals that contain the small polaron and the free electron, respectively. In each case $G = U - TS^{\text{vib}} + PV$. In this relation, U is the internal energy which is the sum of the 0 K DFT energy and the vibrational energy inclusive zero-point energy, S^{vib} is the vibrational entropy, and V is the equilibrium volume. Contributions from other entropies are discussed separately. U, S^{vib}, and V are all functions of T and P determined through the quasiharmonic approximation. In addition, since pressure is related directly to hydrostatic stress, the two terms are used interchangeably here. QHA dynamical matrices for perfect crystal, small polaron, and free electron were calculated using frozen phonon approximation with the aid of the code PHONOPY [38]. We note that $G_{\text{self-trap}}$ is a purely thermodynamic quantity that does not include any notion of activation barriers. As such it cannot help in deciding whether the higher free-energy state coexists with the lower free-energy state. Only the predominance of the low free-energy state can be ascertained based on $G_{\text{self-trap}}$. In this work,$G_{\text{self-trap}}$ is a faithful representation for the polaronic stability at the concentration and defect order in the computational supercells from which it is derived. It is also our best computationally affordable approximation for the dilute limit small polaron stability. More details, including a comparison with hybrid functional calculations of 0 K electron and hole self-trapping energies, are provided in the Supplemental Material (SM) [39].

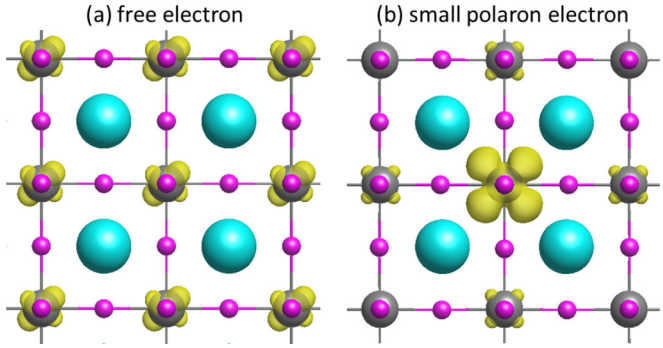

FIG. 1. Visualization of a spin density isosurface, shown in yellow, of (a) a free electron taken at $0.0018\,e/\text{Å}^3$ and (b) a small polaron taken at $0.0030\,e/\text{Å}^3$. For illustration purposes only, the free-electron spin density was generated using a low accuracy single k point. Accurate calculations used for the rest of the work do not yield a net spin for the free electron inside the PAW sphere. Blue (large), gray (medium), and magenta (small) balls represent Sr, Ti, and O, respectively. Visualization rendered with the software VESTA [40].

The bottom of the conduction band of $SrTiO_3$ is composed of Ti t_{2g} states. A free electron partially occupies these states, as schematically shown in Fig. 1(a). An electron small polaron occupies an in-gap state derived from a d_{xy}-like orbital, and is localized on a single Ti ion to result in Ti^{3+} as shown in Fig. 1(b).

Figure 2(a) depicts the resulting T-P predominance map of these two electronic defects in $SrTiO_3$, based on $G_{\text{self-trap}}$ which is expressed in units of meV in Fig. 2(b). It is insightful to first examine other thermodynamic potentials of self-trapping separately and sequentially, from Figs. 2(c) to 2(e), with the understanding that ultimate predominance is decided by $G_{\text{self-trap}}$. Before discussing these maps, we clarify their boundaries in the T-P space. The largest accessible tensile strain at 0 K is 0.035 in ⟨001⟩, beyond which an optical zone center phonon softens (SM Fig. S4 [39]). Thus, two equations of state are needed to describe the crystal: one below and one above this critical strain. Here we restrict the analysis to strains below 0.035. The largest accessible compressive strain at 0 K is 0.010 in ⟨001⟩, beyond which it is not possible to stabilize the small polaron solution in DFT. The black dashed lines in all panels of Fig. 2 point to the experimental boundary between the cubic and tetragonal phases of $SrTiO_3$ [41]. The highest temperature (1000 K) is chosen to remain within the range of validity of the QHA, since the corresponding thermal energy is less than the energy of the fastest vibrational mode at the largest tensile strain considered here.

With those boundaries in place, if we limit the comparison of stability between the free electron and small polaron to only the internal energy (U) as in Fig. 2(c), then the free electron predominates except at high temperature mainly in the tensile zone, where the small polaron is dominant due to its vibrational energy U^{vib}. Next, Fig. 2(d) shows that, based on Helmholtz free energy of self-trapping, the free

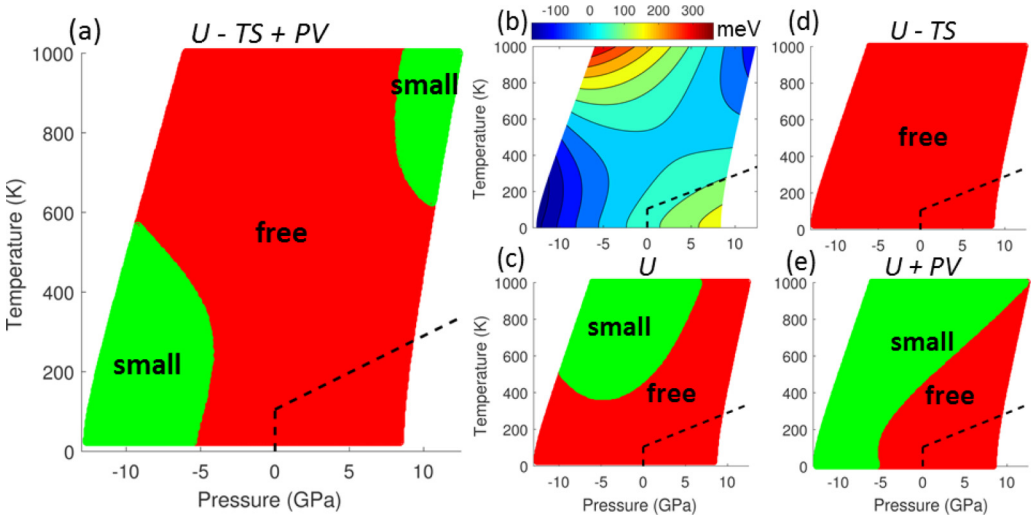

FIG. 2. (a) Predominance map of electronic defects as a function of temperature and pressure in cubic $SrTiO_3$ calculated quasiharmonically based on self-trapping Gibbs free energy. (b) $G_{\text{self-trap}}$ in meV as a function of T and P corresponding to the map in (a). Predominance maps based on other thermodynamic potentials are shown in (c) internal energy, (d) Helmholtz free energy, and (e) enthalpy. In (a), (c), (d), and (e) green and red indicate small polaron and free-electron predominance zones, respectively. The black dashed line in all panels represents the experimental boundary between the cubic and tetragonal phases of $SrTiO_3$ from Ref. [41]. Cubic $SrTiO_3$ is stable above the boundary.

electron is always more stable. In the tensile zone, S^{vib} promotes stabilization of the free electron, thus concealing the role played by U^{vib} in stabilizing the small polaron in Fig. 2(c). However, in the compressive zone the small polaron does in fact generate more S^{vib} but this is not enough for it to predominate. These observations are corroborated by explicit calculation of S^{vib} of formation for both defects in SM Fig. S5 [39]. The predominance map based on the enthalpy of self-trapping is shown in Fig. 2(e). Under tensile hydrostatic stress where $P < 0$, a larger positive relaxation volume Ω of the defect implies a greater minimization of the enthalpy (and hence Gibbs energy). Conversely, a smaller positive Ω would be preferred under compressive stress where $P > 0$. As we present below, Ω for both of the electronic defects is positive throughout this T-P space, but the small polaron exhibits a larger Ω at low T tensile stress and a smaller Ω at high T compressive stress compared to the free electron. Consequently, the new predominance zones of the small polaron that appear in Fig. 2(e) on top of those already present in Fig. 2(c) can be explained by the PV term.

The resulting predominance map in Fig. 2(a) illustrates the coupling between these electronic defects and thermomechanical forces based on $G_{\text{self-trap}}$. First, we note that at $P = 0$, we do not observe a transition at $\Theta_D/2$ from a free electron at low T to a small polaron at high T. This is in accordance with experiments [10] but in contrast to the Holstein model [2]. That model is insightful, but its simplifying assumptions of a one-dimensional crystal and one phonon mode do not capture the complexity of $SrTiO_3$. Second, the predominance zone of the small polaron under tensile stress and low temperature is due chiefly to the PV term for which the small polaron has larger Ω. Last, the predominance zone of the small polaron under compressive stress and high temperature is due to the synergy between the PV and $-TS$ terms. In Fig. 2(b) we show the magnitude $G_{\text{self-trap}}(T, P)$. This graph shows that T and P can vary $G_{\text{self-trap}}$ between -180 meV and $+360$ meV. In SM Fig. S6 [39], we provide the magnitude of self-trapping based on other thermodynamic potentials. This rich thermodynamic picture revealed by the QHA would be overshadowed if analysis was restricted only to 0 K and/or constant volume investigations (SM Sec. 5 [39]).

The dependence of Ω on T and P has far-reaching implications that do not appear to have been considered for electronic defects in semiconductors [18,42] such as $SrTiO_3$. In Figs. 3(a) and 3(b), we show Ω for free electron and small polaron as a function of T and P. The positivity of Ω for both defects indicates that both lead to lattice expansion, which is also known as chemical expansion [43]. Moreover, on an isotherm, Ω increases from compressive to tensile stress for both defects as would be expected intuitively. In addition, $(\partial\Omega/\partial T)|_P > 0$ for both defects, except for the small polaron

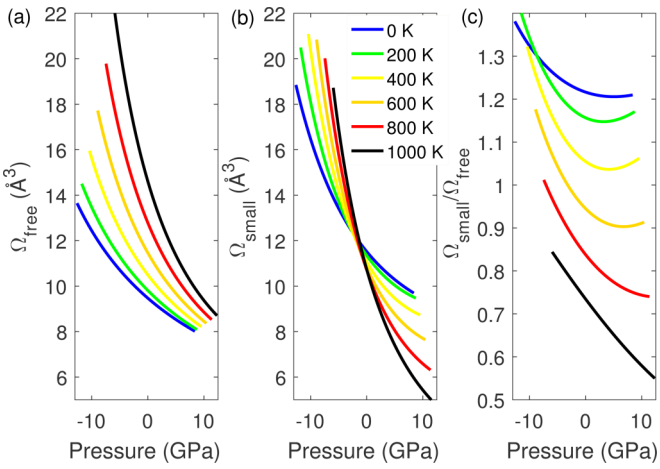

FIG. 3. Pressure dependence of relaxation volume Ω isotherms for (a) free electron and (b) small polaron. (c) The ratio of the relaxation volumes of both defects as a function of T and P.

at stresses exceeding −2 GPa. The most intriguing observation is the temperature dependence of the ratio of the two relaxation volumes, shown in Fig. 3(c).

At 0 K, $\Omega_{small} > \Omega_{free}$, consistent with the notion that charge localization leads to larger chemical expansion [44,45]. However, $(\partial\Omega_{small}/\partial T)|_P < (\partial\Omega_{free}/\partial T)|_P$ and as such there is a transition temperature (that depends on pressure) above which the free electron exhibits a larger Ω than the small polaron. This result implies that $(\partial V_{small}/\partial T)|_P < (\partial V_{free}/\partial T)|_P$ where V is the volume of the crystal containing the electronic defect. In other words, the thermal expansion of $SrTiO_3$ with a small polaron is smaller than the thermal expansion of $SrTiO_3$ with a free electron (see SM Fig. S9 [39]). The origin of this feature can be understood via a Maxwell relation to obtain $(\partial S_{small}/\partial P)|_T > (\partial S_{free}/\partial P)|_T$, which indicates that upon finite isothermal expansion the small polaron generates less entropy than the free electron (see SM Sec. 7 [39]). Since only S^{vib} is considered here, we rationalize this result by observing that the free electron is uniformly spread over Ti ions, and thus it leads to uniform expansion of all cation-anion bonds. This bond loosening lowers the accessible vibrational states at a given temperature and generates more S^{vib}. The localization of the small polaron, however, leads to a complex relaxation pattern around the Ti^{3+} site as schematically shown in Figs. 4(c) and 4(d). Under either hydrostatic tension or compression, with respect to the defect-free crystal the first-neighbor anions are repelled (SM Table S4 [39]). The bonds between these anions and Ti^{3+} exhibit a Jahn-Teller distortion [46] and are relatively elongated and reduced in stiffness [Fig. 4(c), red], which increases S^{vib}. Simultaneously, first-neighbor Ti cations are attracted to the Ti^{3+} site and the bonds between them and first-neighbor anions are shortened [Fig. 4(d), blue], leading to a harder vibrational spectrum and less S^{vib}. The net effect is that the small polaron generates less S^{vib} under finite isothermal expansion. This is exemplified in Figs. 4(a) and 4(b) depictions of phonon density of states at 800 K. The peak spanning 60–80 meV is derived predominantly from oxygen vibrations [47]. Hydrostatic expansion from +3 to 0 GPa left-shifts this peak for both the free electron and small polaron. However, for only the free electron, this entire peak is shifted below $800k_B$ [black vertical line in Figs. 4(a) and 4(b)]. Thus, it is available for phonon occupation at this temperature and pressure. The same peak in the case of the small polaron is broader and part of it is split to form a smaller peak at higher energy. As such, part of it remains above $800k_B$ upon isothermal expansion. The choice of the specific pressures and temperature implemented in Figs. 4(a) and 4(b) is because they clearly illustrate visually a phenomenon that actually affects the full density of states; the integrated effect is reflected in the predominance map of Fig. 2(a) and the overall formation vibrational entropies of both defects as a function of T and P are calculated explicitly in SM Fig. S5 [39]. Clearly, more S^{vib} is generated in the case of the free electron.

The relaxation of the small polaron encompasses both softening and hardening of the vibrational spectrum. Thus, it is anticipated that under tensile stress the softening component dominates, whereas under compressive stress the hardening component takes over. This is the underlying reason for the sign reversal of $(\partial\Omega/\partial T)|_P$ at −2 GPa in Fig. 3(b) and the presence of a corresponding minimum in the small polaron

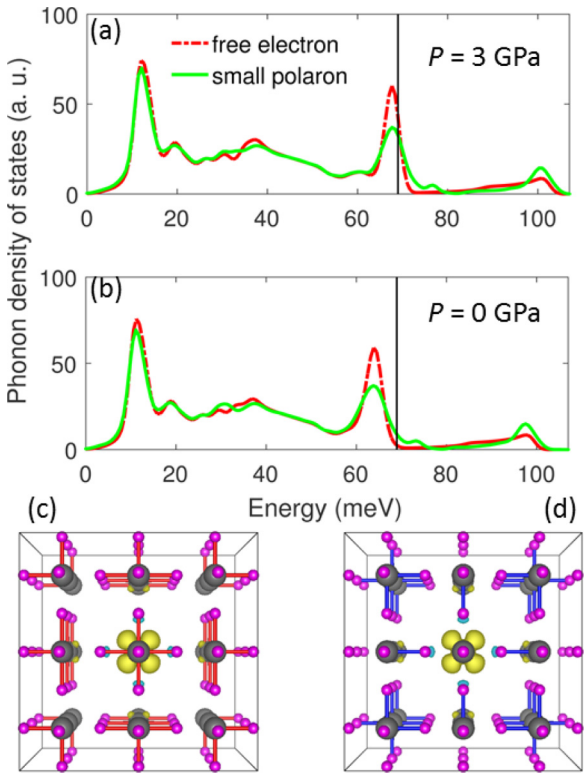

FIG. 4. Phonon density of states in arbitrary units (a.u.) for $SrTiO_3$ containing free electron and small polaron at $T = 800$ K and (a) $P = 3$ GPa and (b) $P = 0$ GPa. These plots were obtained by spline interpolation. The black line represents 800 K in energy units of Boltzmann constant ($800k_B$). Visualizations of the lengthened (red) and shortened (blue) Ti-O bonds around a small polaron are shown in (c) and (d), respectively. Sr ions were removed for clarity and the rest of the color code is the same as in Fig. 1.

formation S^{vib} isotherms in SM Fig. S5(a) [39]. The strong dependence of Ω on T and P presented here in the case of the electronic defects could possibly explain the observed temperature-dependent chemical expansion coefficient in Fe-doped $SrTiO_3$ [48]. Conclusive analysis, however, requires computing $\Omega(T, P)$ for relevant intrinsic and extrinsic defects in doped $SrTiO_3$.

Another utility of our analysis is extraction of the absolute hydrostatic deformation potential of the conduction-band edge a_c from Ω_{free}. Because of the ambiguity in defining pressure in charged defect calculations [18], Ω_{free} was not calculated directly but obtained from a_c [18,19]. The latter is obtained from nontrivial DFT calculations [49]. Here the pressure was obtained unambiguously by fitting the defective crystal energy vs volume to an equation of state, and thus it is possible to directly compute Ω_{free}. From $\Omega_{free}(T = 0, P = 0)$ we obtain a value for a_c of −10.4 eV. It is not possible to validate this prediction given the wide scatter in the suggested values reported to date for a_c in $SrTiO_3$ (−0.33 eV [50] to −15 eV [51]) and the absence of direct experimental measurement [19,50–53]. This new approach to compute a_c offers prediction of T and P dependence of a_c at a low computational cost, but further studies are needed to confirm its accuracy.

Future extensions of this work can investigate the effects of the large anharmonicity of $SrTiO_3$ beyond the QHA [54] and its large LO-TO phonon splittings [55]. We did not account here for concentration-dependent quantities such as the electronic and configurational entropies. These are coupled to other defects via the chemical potential of electrons (Fermi level). Thus, it is not possible to address their effects without accounting for other important point defects in the analysis such as oxygen vacancies (Sec. 9 in SM [39]).

In summary, we combined DFT and the QHA to enable the assessment of the effect of temperature and pressure on charged defects in semiconductors. By applying this approach to $SrTiO_3$, we elucidated the rich thermodynamics underlying the free-energy landscape of free electrons and small polarons. We showed that the combined action of temperature and mechanical stress can tune the relative stability of these electronic defects. We anticipate that the results presented here for electrons in $SrTiO_3$ are applicable for the family of titanate perovskites. In order to deduce the associated electronic conductivity changes, kinetic analyses of stress-dependent mobility and defect coexistence are needed. However, to a first approximation the electronic defect predominance uncovered here can guide the design of optimal thermodynamic functional conditions to promote the desirable form of electronic defects in electronic or electrochemical applications. For example, at a given temperature, mechanical stress can be tuned to promote free electrons in electronics and photoelectrodes to accelerate electronic conductivity. Alternatively, stress can be altered to stabilize small polarons and decelerate electronic conductivity for design of protective corrosion-resistant coatings.

This work was supported primarily by the MRSEC Program of the National Science Foundation (NSF) under Award No. DMR-1419807. We are grateful for the computational support from NSF through the XSEDE Science Gateways program under allocation TG-DMR 140065.

[1] J. Appel, in *Solid State Physics*, edited by D.Turnbull and H. E. Frederick Seitz (Academic, New York, 1968), pp. 193–391.
[2] T. Holstein, Ann. Phys. (NY) **8**, 343 (1959).
[3] A. J. E. Rettie, W. D. Chemelewski, D. Emin, and C. B. Mullins, J. Phys. Chem. Lett. **7**, 471 (2016).
[4] N. V. Skorodumova, S. I. Simak, B. I. Lundqvist, I. A. Abrikosov, and B. Johansson, Phys. Rev. Lett. **89**, 166601 (2002).
[5] M. V. Ganduglia-Pirovano, A. Hofmann, and J. Sauer, Surf. Sci. Rep. **62**, 219 (2007).
[6] C. Gionco, M. C. Paganini, E. Giamello, R. Burgess, C. Di Valentin, and G. Pacchioni, Chem. Mater. **25**, 2243 (2013).
[7] J. F. Schooley, W. R. Hosler, and M. L. Cohen, Phys. Rev. Lett. **12**, 474 (1964).
[8] W. D. Rice, P. Ambwani, M. Bombeck, J. D. Thompson, G. Haugstad, C. Leighton, and S. A. Crooker, Nat. Mater. **13**, 481 (2014).
[9] D. Kan, T. Terashima, R. Kanda, A. Masuno, K. Tanaka, S. Chu, H. Kan, A. Ishizumi, Y. Kanemitsu, Y. himakawa, and M. Takano, Nat. Mater. **4**, 816 (2005).
[10] G. M. Choi, H. L. Tuller, and D. Goldschmidt, Phys. Rev. B **34**, 6972 (1986).
[11] J. L. M. van Mechelen, D. van der Marel, C. Grimaldi, A. B. Kuzmenko, N. P. Armitage, N. Reyren, H. Hagemann, and I. I. Mazin, Phys. Rev. Lett. **100**, 226403 (2008).
[12] A. Fujimori, I. Hase, M. Nakamura, H. Namatame, Y. Fujishima, Y. Tokura, M. Abbate, F. M. F. de Groot, M. T. Czyzyk, J. C. Fuggle, O. Strebel, F. Lopez, M. Domke, and G. Kaindl, Phys. Rev. B **46**, 9841 (1992).
[13] Y. Yamada, H. K. Sato, Y. Hikita, H. Y. Hwang, and Y. Kanemitsu, Phys. Rev. Lett. **111**, 047403 (2013).
[14] T. Kohmoto, D. Ikeda, X. Liang, and T. Moriyasu, Phys. Rev. B **87**, 214301 (2013).
[15] A. Janotti, J. B. Varley, M. Choi, and C. G. Van de Walle, Phys. Rev. B **90**, 085202 (2014).
[16] X. Hao, Z. Wang, M. Schmid, U. Diebold, and C. Franchini, Phys. Rev. B **91**, 085204 (2015).
[17] P. Erhart, A. Klein, D. Åberg, and B. Sadigh, Phys. Rev. B **90**, 035204 (2014).
[18] F. Bruneval, C. Varvenne, J.-P. Crocombette, and E. Clouet, Phys. Rev. B **91**, 024107 (2015).
[19] A. Janotti, B. Jalan, S. Stemmer, and C. G. V. de Walle, Appl. Phys. Lett. **100**, 262104 (2012).
[20] D. Marrocchelli, S. R. Bishop, H. L. Tuller, and B. Yildiz, Adv. Funct. Mater. **22**, 1958 (2012).
[21] B. Yildiz, MRS Bull. **39**, 147 (2014).
[22] S.-Y. Choi, S.-D. Kim, M. Choi, H.-S. Lee, J. Ryu, N. Shibata, T. Mizoguchi, E. Tochigi, T. Yamamoto, S.-J. L. Kang, and Y. Ikuhara, Nano Lett. **15**, 4129 (2015).
[23] A. Kushima and B. Yildiz, J. Mater. Chem. **20**, 4809 (2010).
[24] K. Rim, J. Chu, H. Chen, K. A. Jenkins, T. Kanarsky, K. Lee, A. Mocuta, H. Zhu, R. Roy, J. Newbury, J. Ott, K. Petrarca, P. Mooney, D. Lacey, S. Koester, K. Chan, D. Boyd, M. Ieong, and H. S. Wong, in 2002 Symposia VLSI Technol. Dig. Tech. Pap. Cat. No. 01CH37303, 2002, p. 98.
[25] A. L. Shluger and A. M. Stoneham, J. Phys.: Condens. Matter **5**, 3049 (1993).
[26] S. Baroni, P. Giannozzi, and E. Isaev, Rev. Mineral. Geochem. **71**, 39 (2010).
[27] K. Umemoto, E. Sugimura, S. de Gironcoli, Y. Nakajima, K. Hirose, Y. Ohishi, and R. M. Wentzcovitch, Phys. Rev. Lett. **115**, 173005 (2015).
[28] C. Freysoldt, B. Grabowski, T. Hickel, J. Neugebauer, G. Kresse, A. Janotti, and C. G. Van de Walle, Rev. Mod. Phys. **86**, 253 (2014).
[29] P. E. Blöchl, Phys. Rev. B **50**, 17953 (1994).
[30] G. Kresse and D. Joubert, Phys. Rev. B **59**, 1758 (1999).
[31] G. Kresse and J. Hafner, Phys. Rev. B **47**, 558 (1993).
[32] G. Kresse and J. Hafner, Phys. Rev. B **49**, 14251 (1994).
[33] G. Kresse and J. Furthmüller, Comput. Mater. Sci. **6**, 15 (1996).
[34] G. Kresse and J. Furthmüller, Phys. Rev. B **54**, 11169 (1996).
[35] J. P. Perdew, A. Ruzsinszky, G. I. Csonka, O. A. Vydrov, G. E. Scuseria, L. A. Constantin, X. Zhou, and K. Burke, Phys. Rev. Lett. **100**, 136406 (2008).

[36] S. L. Dudarev, G. A. Botton, S. Y. Savrasov, C. J. Humphreys, and A. P. Sutton, Phys. Rev. B **57**, 1505 (1998).
[37] S. Lany and A. Zunger, Phys. Rev. B **80**, 085202 (2009).
[38] A. Togo, F. Oba, and I. Tanaka, Phys. Rev. B **78**, 134106 (2008).
[39] See Supplemental Material at http://link.aps.org/supplemental/10.1103/PhysRevB.95.161110 for supplemental methods, soft normal mode, vibrational entropy, self-trapping potentials, and thermal expansion of defective and perfect $SrTiO_3$.
[40] K. Momma and F. Izumi, J. Appl. Crystallogr. **44**, 1272 (2011).
[41] M. Guennou, P. Bouvier, J. Kreisel, and D. Machon, Phys. Rev. B **81**, 054115 (2010).
[42] S. Grieshammer, T. Zacherle, and M. Martin, Phys. Chem. Chem. Phys. **15**, 15935 (2013).
[43] S. R. Bishop, D. Marrocchelli, C. Chatzichristodoulou, N. H. Perry, M. B. Mogensen, H. L. Tuller, and E. D. Wachsman, Annu. Rev. Mater. Res. **44**, 205 (2014).
[44] D. Marrocchelli, S. R. Bishop, H. L. Tuller, G. W. Watson, and B. Yildiz, Phys. Chem. Chem. Phys. **14**, 12070 (2012).
[45] N. H. Perry, S. R. Bishop, and H. L. Tuller, J. Mater. Chem. A **2**, 18906 (2014).
[46] G. Corradi, I. M. Zaritskii, A. Hofstaetter, K. Polgár, and L. G. Rakitina, Phys. Rev. B **58**, 8329 (1998).
[47] N. Choudhury, E. J. Walter, A. I. Kolesnikov, and C.-K. Loong, Phys. Rev. B **77**, 134111 (2008).
[48] N. H. Perry, J. J. Kim, S. R. Bishop, and H. L. Tuller, J. Mater. Chem. A **3**, 3602 (2015).
[49] C. G. Van de Walle and R. M. Martin, Phys. Rev. Lett. **62**, 2028 (1989).
[50] M. Stengel, Phys. Rev. B **92**, 205115 (2015).
[51] C. S. Koonce, M. L. Cohen, J. F. Schooley, W. R. Hosler, and E. R. Pfeiffer, Phys. Rev. **163**, 380 (1967).
[52] A. N. Morozovska, E. A. Eliseev, G. S. Svechnikov, and S. V. Kalinin, Phys. Rev. B **84**, 045402 (2011).
[53] A. M. Dehkordi, S. Bhattacharya, T. Darroudi, H. N. Alshareef, and T. M. Tritt, J. Appl. Phys. **117**, 055102 (2015).
[54] T. Tadano and S. Tsuneyuki, Phys. Rev. B **92**, 054301 (2015).
[55] W. Zhong, R. D. King-Smith, and D. Vanderbilt, Phys. Rev. Lett. **72**, 3618 (1994).